

Flexural performance of cold-formed square CFST beams strengthened with internal stiffeners

Ahmed W. Al Zand^{*1}, W.H. Wan Badaruzzaman^{*1}, Mustafa M. Ali¹,
Qahtan A. Hasan¹ and Marwan S. Al-Shaikhli²

¹Smart and Sustainable Township Research Centre, Universiti Kebangsaan Malaysia (UKM), Selangor, Malaysia
²Civil Engineering Department, Madenat Alelem University College, Baghdad, Iraq

(Received July 29, 2019, Revised October 16, 2019, Accepted October 21, 2019)

Abstract. The tube outward local buckling of Concrete-Filled Steel Tube (CFST) beam under high compression stress is still considered a critical problem, especially for steel tubes with a slender section compared to semi-compact and compact sections. In this study, the flexural performance of stiffened slender cold-formed square tube beams filled with normal concrete was investigated. Fourteen (14) simply supported CFST specimens were tested under static bending loads, stiffened with different shapes and numbers of steel stiffeners that were provided at the inner sides of the tubes. Additional finite element (FE) CFST models were developed to further investigate the influence of using internal stiffeners with varied thickness. The results of tests and FE analyses indicated that the onset of local buckling, that occurs at the top half of the stiffened CFST beam's cross-section at mid-span was substantially restricted to a smaller region. Generally, it was also observed that, due to increased steel area provided by the stiffeners, the bending capacity, flexural stiffness and energy absorption index of the stiffened beams were significantly improved. The average bending capacity and the initial flexural stiffness of the stiffened specimens for the various shapes, single stiffener situations have increased of about 25% and 39%, respectively. These improvements went up to 45% and 60%, for the double stiffeners situations. Moreover, the bending capacity and the flexural stiffness values obtained from the experimental tests and FE analyses validated well with the values computed from equations of the existing standards.

Keywords: slender tube section; CFST beam; internal stiffeners; buckling failure; stiffening; cold-formed tube

1. Introduction

The composite members known as the Concrete-Filled Steel Tube (CFST) are increasingly adopted in two-point projects (Han *et al.* 2014). In addition to the ductility and strength capacity improvements, they can reduce the cost of a project by reducing the construction time, the amount of workmanship and eliminating the cost of formworks. In the last two decades, several studies have extensively investigated the performance of CFST columns regarding the type of infill material, the compressive strength of concrete, steel tube shapes, double skin tubes and the type of loading (dynamic or static). Examples of such studies are presented by (Han *et al.* 2001, Han *et al.* 2006a, Yang and Han 2006, Bahrami *et al.* 2011, Qian *et al.* 2011, Bahrami *et al.* 2012, Abdalla *et al.* 2013, Yang and Ma 2013, Yang 2015, Hassan *et al.* 2016, Ekmekyapar and Al-Eliwi 2017, Chen *et al.* 2018, Liang *et al.* 2018, Lu *et al.* 2018, Lu *et al.* 2018, Hosseinpour *et al.* 2018).

To identify whether the tubular cross-sections are liable to local buckling or not, several design standards of tubular

steel members provide steps to classify their cross-sections into different groups. This classification is dependent on the dimensions, thickness and the yielding strength of steel tube section. The Eurocode 3 for the Design of Steel Structures (EC3 (2002)) has classified these tubular sections as Classes 1, 2, 3 or 4. Meanwhile, both of the American Institute of Steel Construction (AISC (1999)) and Australian Standard (AS 4100 (1998)) have classified these tubular sections as Compact, Non-compact or Slender (Zhao and Jaspert 2005).

Typically, in a CFST composite system, the infill concrete material can sufficiently prevent the inward local buckling failure that occurs in the steel tube's wall when it is subjected to high compression stress. However, it cannot prevent outward local buckling (Han *et al.* 2014). Increasing the steel tube thickness to avoid such a phenomenon is considered an uneconomic solution since the self-weight of steel material will increase accordingly. Thus, researchers have investigated the influence of using additional steel stiffeners for the steel tubes of CFST columns that have sufficient embedded length for bonding with the concrete core (Huang *et al.* 2002, Tao *et al.* 2007, Chen and Jin 2010, Bahrami *et al.* 2011, Lee *et al.* 2011, Bahrami *et al.* 2013, Bahrami *et al.* 2014, Ling *et al.* 2014, Hilo *et al.* 2015, Zhu *et al.* 2017, Liang *et al.* 2018, Zhang *et al.* 2019, Yuan *et al.* 2019). Providing these stiffeners demonstrated that they could perfectly restrict the tube's outward local buckling, which leads to a substantial increase in the CFST column's capacity.

*Corresponding authors, Ph.D. Professor,

E-mail: wanhamidon@ukm.edu.my

**Ph.D.

E-mail: ahmedzand70@gmail.com

Furthermore, for unstiffened CFST composite beams that are subjected to a pure flexural loading, the outward tube's local buckling typically occurs at the top half of the beam's cross-section (the zone with high compressive stress), which is highlighted in several studies (Helena and Knight 2005, Han *et al.* 2006b, Guler *et al.* 2012, Jiang *et al.* 2013, Sundararaja and Prabhu (2013), Han *et al.* 2014, Wang *et al.* 2014, Wang *et al.* 2014; Al-Zand *et al.* 2017, Zhu *et al.* 2017, Lu *et al.* 2017, Al Zand *et al.* 2018, Javed *et al.* 2018, Song *et al.* 2019). According to studies in which the performance of CFST beams was investigated, the outward local buckling failures in steel tubes that have a cross-section classified as a compact section (Class 1) are highly limited compared to the thinner tube sections which are classified as semi-compact and slender sections (Class 2 to 4). To date, very limited researches have been conducted concerning the stiffening performance of the steel tubes of CFST beams, which is required for preventing or delaying outward local buckling failure. For example, Kang *et al.* (2007) have investigated the use of mechanical interlocking stiffeners to improve the composite action between the circular steel tube and the concrete core, which were applied along the inner face of the steel tube and have effectively improved the loading capacity and ductility of the tested CFST beams. Recently, the performance of square CFST beams that are externally retrofitted from either the bottom side only or from the top and bottom sides by flat steel plates (connected by mechanical bolts) was experimentally studied by AL-Shaar and Göğüş (2018). The moment capacities of the retrofitted CFST beams from both the top and bottom sides were enhanced by about 45%.

However, the above existing studies have only investigated the stiffening performance of CFST beams that have compact and semi-compact tube sections, whereas, stiffening the CFST beams with a slender tube section has not yet been investigated. Slender steel tubes are cheaper than compact sections. Even though there will be additional cost coming from the steel stiffeners, on the overall, but still this is more economical than increasing the steel tube cross-sectional area. This is due to the stiffeners' ability to control the steel buckling failure, and hence resulting in a higher loading capacity for the CFST member (Zhu *et al.* 2017).

Therefore, the current study investigates the influence of using internal steel plate stiffeners that can delay or restrict the local buckling of slender cold-formed steel tubes that are filled with normal concrete (CFST beams). These newly suggested stiffeners should be provided at each inner side of the tube's cross-section with various shapes (I, T and V) and number (single and double), and expected to be sufficiently bonded with the concrete of the CFST beams. Varied stiffened CFST specimens with a high w/t ratio were tested under four-point loading, included two (2) specimens tested without stiffening action, which can be considered as control specimens. Finite element (FE) analyses were adopted to develop additional CFST models using the ABAQUS software in order to investigate another parameter that was not experimentally investigated. The failure modes, energy absorption capability, flexural stiffness and bending capacity of the tested CFST beams are extensively discussed in this study. Furthermore, the

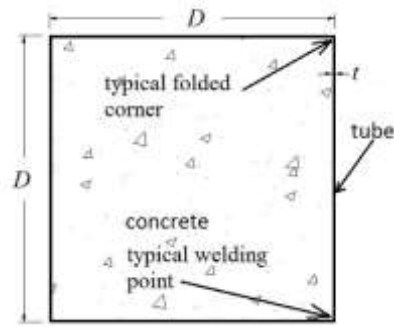
bending capacity and the flexural stiffness values obtained from the current test and FE analyses validated with the computed values using the existing theoretical methods and code standards.

2. Experimental work

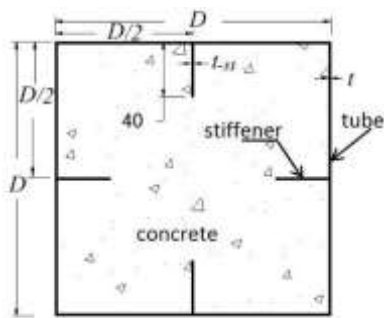
2.1 Numerical simulation procedure

Fourteen (14) simply supported CFST specimens were tested in the current study under pure static bending load. The specimens were classified into two groups: seven (7) specimens with an effective length (support-to-support; L_e) of 1,050 mm were designated as short beams (SB), and another seven (7) specimens of length 2,150 mm were designated as long beams (LB). A steel plate with a thickness t of 1.5 mm was used to fabricate the square tube cross-sections with outside dimensions (D for depth and width) of 200 mm. With these dimensions and thickness, the *width/thickness* ratio is equal to 131.3. Therefore, according to the requirements of AISC (1999), the suggested tube's section can be classified as a slender section. Using the same steel tube plate thickness (1.5 mm), three shapes of internal steel stiffeners ($t_{s,i}$) were provided along the full lengths of the inner steel tube's sides. First, the steel stiffeners were separately fabricated and welded at their designed locations on a flat steel plate, after which, the latter was carefully folded by a press machine to achieve the suggested square shape of cold-formed square steel tube. The square-shaped tube was fabricated by folding the flat steel plate into three folded sides. To complete the tube, the one remaining corner was formed by fully welding a flat steel plate onto the open edges along the already folded plate using Metal Inert Gas (MIG) welding machine. Figure 1 presents the schematic diagram of the suggested CFST specimens' cross-sections (all dimensions are specified in mm). Eight (8) mm square-shaped steel plate cut to the same dimensions of the hollow tube was welded to one end of each tube specimen, thus covering the opening on one end. The tubes were placed vertically standing on their closed-end at their base during concreting. Concrete was poured from the top opened end, and an electrical vibrator was used to vibrate the concrete infill to prevent cavities inside the tubes from forming during the casting work.

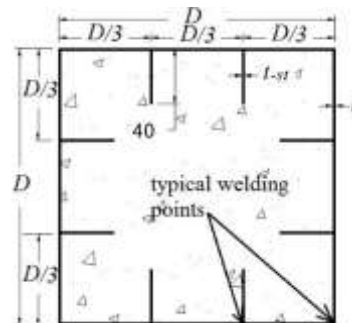
The designations and properties of specimens are listed in Table 1. For each group of specimens (SB and LB), a tube was fabricated without internal stiffeners and was considered to be the control specimen (SB1-C/LB1-C), as shown in Fig. 1(a). For the stiffened CFST specimens, single or double steel stiffeners were provided at each internal side of the steel tube. Three (3) different shapes of stiffeners were suggested in the current research work aimed at investigating the efficiency of their bonding with the concrete infill. These shapes are I-shape, T-shape and V-shape (see Fig. 1). The outer dimensions of all suggested square specimens are 200 mm x 1.5 mm ($D \times t$). During the test, the welded corner of all specimens was placed at the bottom side (at the tension zone).



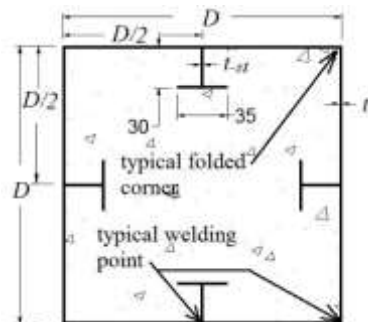
(a) Control (C)



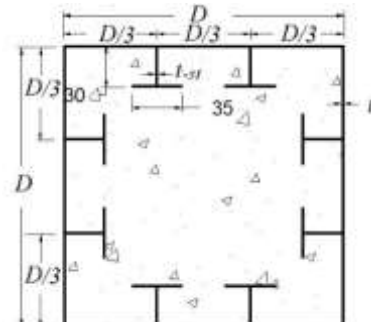
(b) Single I-shape (SI)



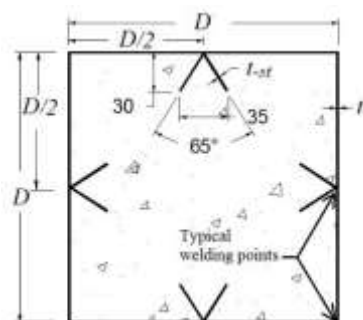
(c) Double I-shape (DI)



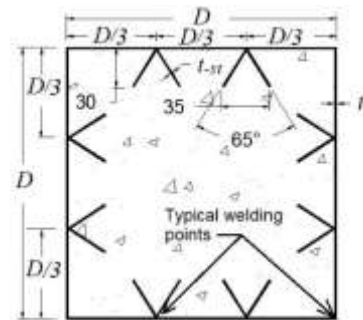
(d) Single T-shape (ST)



(e) Double T-shape (DT)



(f) Single V-shape (SV)



(g) Double V-shape (DV)

Fig. 1 Cross-section schemes of CFST specimens with different shapes of internal stiffeners

Table 1 Specimens designation and properties

Short /Long Specimens	Stiffeners at each wall's side	t and t_{st} (mm)	f_{cu} (MPa)	f_y (MPa)	A_s $\times 10^3$ (mm ²)	I_s $\times 10^7$ (mm ⁴)	A_c $\times 10^4$ (mm ²)	I_c $\times 10^8$ (mm ⁴)	ζ
LB1 / SB1-C	-	1.5	45.1	346	1.19	0.78	3.88	1.26	0.35
LB2 / SB2-SI	Single I-shape	1.5	45.1	346	1.42	0.86	3.86	1.25	0.35
LB3 / SB3-DI	Double I-shape	1.5	45.1	346	1.65	0.96	3.83	1.24	0.35
LB4 / SB4-ST	Single T-shape	1.5	45.1	346	1.57	0.90	3.84	1.24	0.35
LB5 / SB5-DT	Double T-shape	1.5	45.1	346	1.95	1.05	3.81	1.23	0.35
LB6 / SB6-SV	Single V-shape	1.5	45.1	346	1.57	0.92	3.84	1.24	0.35
LB7 / SB7-DV	Double V-shape	1.5	45.1	346	1.95	1.10	3.80	1.22	0.35

Table 2 Physical properties of the steel plates

t and t_{st} (mm)	f_y (MPa)	ϵ_y (%)	f_u (MPa)	ϵ_{su} (%)	E_s (GPa)	ϵ_{sr} (%)
1.5	346	0.44	432	12.6	198.2	22.5

2.2 Material properties

The physical properties of the steel plate, which was used to fabricate the suggested cold-formed tube cross-sections and their stiffeners were identified via a direct tensile test. Three coupons were cut and prepared following the requirements of ASTM-E8/8M. Table 2 lists the physical properties of the steel plate on which the test was conducted, such as the yield tensile strength (f_y), yield strain (ϵ_y), ultimate tensile strength (f_u), ultimate strain (ϵ_{su}), modulus of elasticity (E_s), and maximum elongation (ϵ_{sr}).

The components of the concrete mix (cement, sand, coarse aggregate and water) were designed by weight ratio. The concrete mix proportions were as follows: 400kg/m³ cement: 710 kg/m³ sand: 1060 kg/m³ coarse aggregate: 180 kg/m³ water: and chemical superplasticiser type Real Flow 611 with 250 ml/100kg of cement. A 10 mm maximum aggregate size was used in this mixture. The compressive strength, according to the average results over three cubes (150 mm) that were tested at 28 days, was equal to 38.8 MPa. Due to unavoidable circumstances, all specimens were tested after a few months from the casting day. However, three untested concrete cubes were available for the compression test on the same day of testing the specimens. These cubes were cured under the same conditions as the CFST specimens (roof covered and at room temperature). The average concrete compressive strength on the day of specimen testing was equal to 45.1 MPa.

2.3 Test setup

A four-point load was applied to induce pure flexural bending by using a manual hydraulic jack. To measure the change in the specimen's deflection during the test, three (3) linear variable displacement transducers (LVDTs) were distributed equally underneath the beam's length. At the mid-span of various samples (SB1/LB1, SB2/LB2, SB4/LB4 and SB6/LB6), four (4) strain gauges were provided at the surface of the steel tubes for measuring the

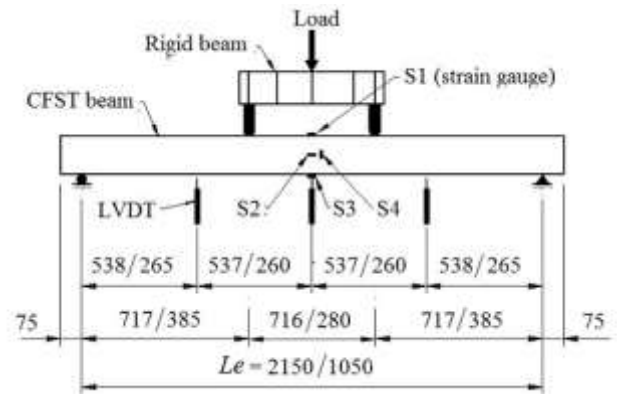


Fig. 2 Test setup scheme for the long beam / short beam

tensile and compression strains. The load was applied gradually with an increment of 4-6 mm/min. The data recorded from the load cell, LVDTs and strain gauges during the test were saved by a computerised data acquisition system (data logger). The schematic diagram of the test setup is presented in Fig. 2 (all dimensions in mm).

3. Results and discussion

3.1 Failure modes

To investigate the behaviour of the CFST specimens, the testing load was applied beyond the specimen's ultimate capacity. Some of the tested specimens were loaded until their bottom steel flange has fractured due to the high tensile stresses, which was occurred mostly for the short specimens. While no steel fracture have been recorded for the specimens with longer span. Thus, their test was stopped when the LVDTs reached its maximum limit (80 mm). The tested specimens (SB2-SI and LB1-C) with short and long lengths are shown in Fig. 3, as an example. No substantial changes were recorded in the cross-section of the control specimens (unstiffened CFST

specimens) until they reached approximately 70-75% of their ultimate load capacities, at which the top flanges of their steel tubes began to buckle outside due to the high compression stresses at a distance between the two-point loads. On the other hand, the top flanges of the specimens with internal stiffeners started to buckle when their loads reached 80-85% of their ultimate load capacities. This is because the internal stiffeners have restricted the outward local buckling of the stiffened tubes to several smaller and separated zones. The top flange of the control specimen (without internal stiffeners) has buckled along the full width of its cross-section, whereas in the case of the stiffened specimens, it only buckled along the distances between the stiffener locations and tube edges, as shown in Fig. 4. The provided internal stiffeners were perfectly welded with steel tube surface and sufficiently bonded with the infilled concrete since even at the maximum loading stage, no vertical slip failure was recorded at the maximum bending zone. Mainly, the shapes of the internal steel stiffeners did not affect the local buckling behaviour of the steel tube. The buckling shape was mainly affected by the number of stiffeners that had been provided at each of the tube's side (see Figs. 4 and 5 for an example). Figure 6 presents a schematic diagram of the typical outward local buckling failure that occurred at the top half of the steel tube's cross-section when the specimen reached their ultimate bending moment, specifically at a distance between the two-point loads. This figure illustrates the positions of the neutral axis (N.A) and the centre line of the cross-section (C.C). All specimens deflected smoothly during the loading stages until reaching their bending capacities, which behaved similar to half-sine curves (Figs. 7 and 8).

3.2 Moment-curvature relationships

The moment vs curvature at mid-span relationships of the tested specimens are discussed in this section. The curvature (φ) values are estimated via the relation between the specimen's effective length and the deflection at mid-span ($\varphi = u_m (\pi / L_e)^2$). This formula is applicable to beams with a half-sine deflection curve (Han 2004, Al Zand *et al.* 2018, Javed *et al.* 2018). The moment vs curvature relationships are presented in Fig. 9 for both tested groups (long and short beams). At the initial loading stage, all CFST specimens exhibit an elastic behaviour followed by an inelastic behaviour until reaching their ultimate moment capacities. Generally, the CFST specimens that have single internal stiffeners exhibit stiffer behaviour in the elastic range than the corresponding control specimens (SB1-C and LB1-C), thereby realising a higher moment capacity. The specimens that have double internal stiffeners exhibit a stiffer performance than both the corresponding control specimens and the specimens with a single stiffener. This is due to that the steel stiffeners have effectively increased the A_s as obviously shown in Table 1.

Furthermore, the long specimens (LB) are more ductile than short specimens. Thus, they did not show any peak load's value (see Fig. 9(b)). Besides, the tests of LB specimens were stopped at the deflection value of 80 mm (LVDT's limitation). Also, they were rested on roller supports which is allowed to slightly slip along their longitudinal direction without much restriction.

The moment vs strain relationships of the tested CFST specimens are presented in Fig. 10. The strain gauges' numbering and locations are described earlier in Section 2.3. Typical flexural behaviour of the simply supported beams was recorded for the tested specimens: as the loading rose, the tensile strain at the bottom flange has gradually increased (positive value of S3), and the compression strain at the top flange has also increased (negative value of S1). From Fig. 10, at the mid-depth of each specimen's cross-section, the tensile strain (S2) began to increase slightly before the specimen reached its ultimate moment value; thus, the N.A, which was located along the centre line of the C.C prior to loading, began to move upward due to the high bending stress (as illustrated earlier in Fig. 6). Furthermore, the steel stiffeners have enabled the same tensile strain limit to be realised with a higher loading value, according to a comparison of the S3 values of the stiffened specimens with their control specimens, as presented in Fig. 11.

3.3 Moment carrying capacity

For all tested CFST specimens, the moment capacity (M_u) is obtained either at the ultimate moment value that was recorded from the loading curve before it began to descend due to the sudden failure that occurred in short specimens, or at the deflection limit which is equal to $L_e/40$ (Javed *et al.* 2018), whichever is higher. For both groups (beams with long and short spans), each specimen that had a single stiffener reached a higher M_u value than the corresponding control specimen, and each specimen that had double stiffeners reached a higher value than all other corresponding specimens, as presented in Table 3. This is expected since the provided steel stiffeners led to increasing the cross-sectional area (A_s) of the steel tube (see Table 1). The moment improvement percentage (MIP) of the stiffened specimens was estimated from the M_u value of the corresponding control specimen (unstiffened specimen) for each group separately. For example, the value of M_u of following SB1-C is equal to 45.9 kN.m, and the incorporation of single internal stiffeners has increased the value of M_u to 60.7 kN.m, 58.7 kN.m, and 59.3 kN.m for specimens SB2-SI, SB4-ST, and SB6-SV, respectively, thereby achieving a MIPs of +32.3%, +27.9%, and +29.1%. Then, the use of double internal stiffeners has led to a further enhancement in the M_u value to 65.2 kN.m (+42.1%), 68.3 kN.m (+48.8%), and 69.0 kN.m (+50.2%) for specimens SB3-DI, SB5-DT, and SB7-DV, respectively. The same behaviour was recorded for the long specimens but with slightly lower M_u values than those of shorter specimens, which demonstrates that the longer specimens remain within the plastic failure zone.

The adequacy of the current experimental results was examined. The M_u values that were obtained from the tests have been validated against the theoretically predicted values of two commonly used methods in this field: EC4 (2004) and Han (2004). The details of these methods are as follows

$$M_{u-EC4} = (W_{pa} - W_{pan})f_y + 0.5(W_{pc} - W_{pcn})f_{ck} \quad (1)$$

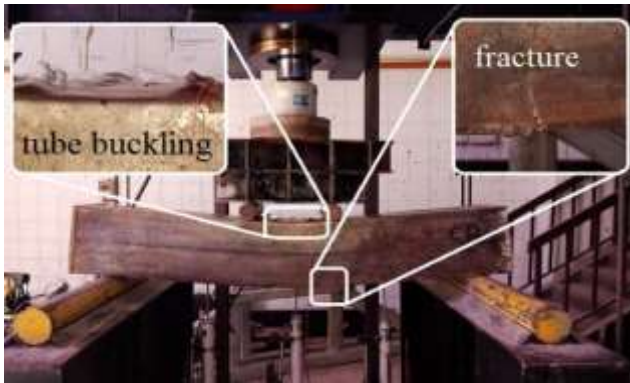
$$h_n = (A_c f_{ck}) / ((2Df_{ck}) + 4t(2f_y - f_{ck})) \quad (2)$$

$$W_{pc} = 0.25.(D - 2t)^3 \quad (3)$$

$$W_{pan} = Dh_n^2 - W_{pcn} \quad (6)$$

$$W_{pcn} = (D - 2t)h_n^2 \quad (4)$$

$$W_{pa} = 0.25D^3 - W_{pc} \quad (5)$$



(a) SB2-SI



(b) LB1-C

Fig. 3 Tested CFST specimens beyond their load's capacities



Fig. 4 Top flange local buckling failure for the tested CFST specimens

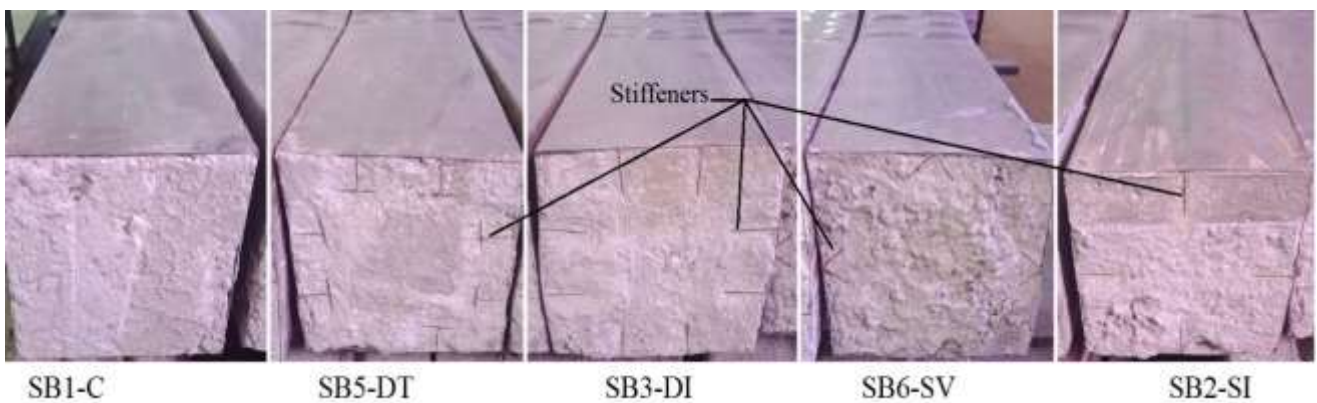
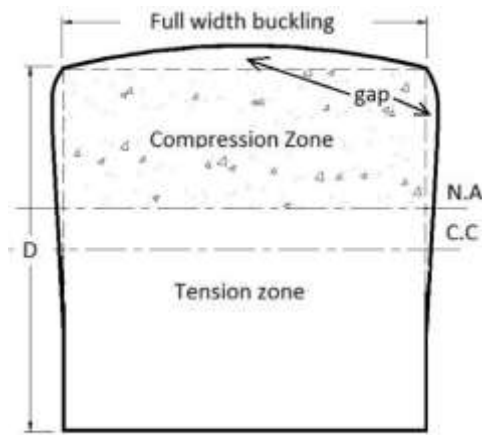
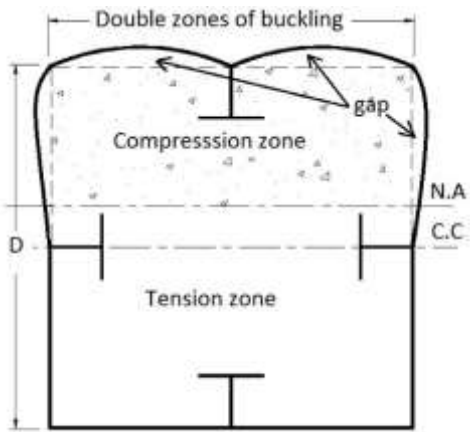


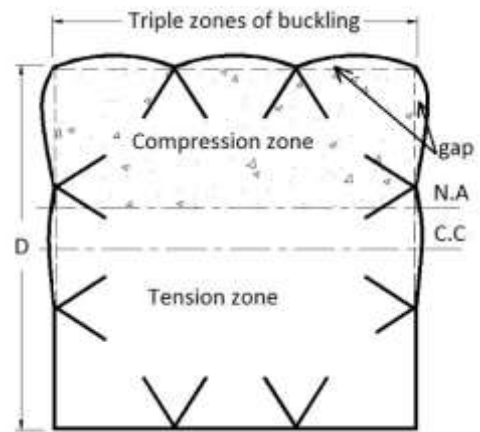
Fig. 5 The CFST cross-sections at the specimens' open ends after the test



(a) Without stiffeners (C)

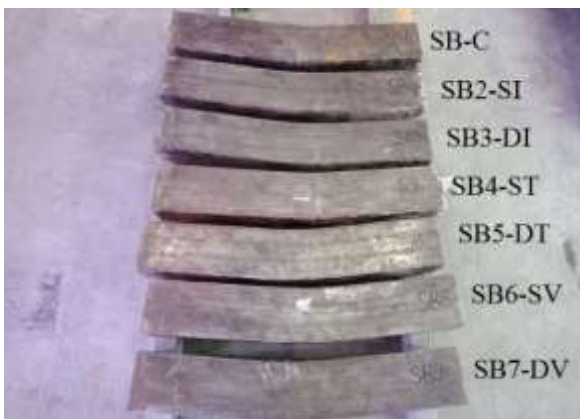


(b) Single stiffener T-shape (ST)



(c) Double stiffener T-shape (DT)

Fig. 6 Scheme of the typical tube outward buckling failure for the tested specimens



(a) Short specimens



(b) Long specimens

Fig. 7 The bending behaviour of all tested specimens

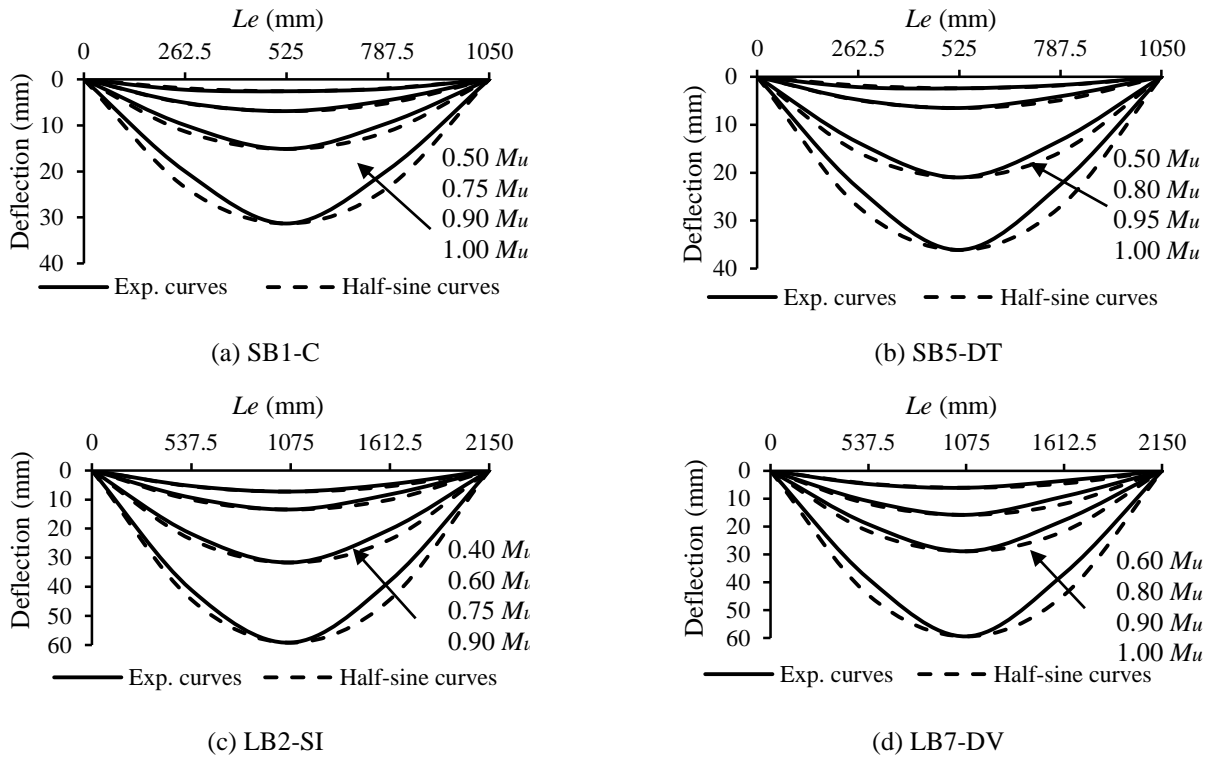


Fig. 8 Typical deflection shape of the tested specimens during varied loading stages

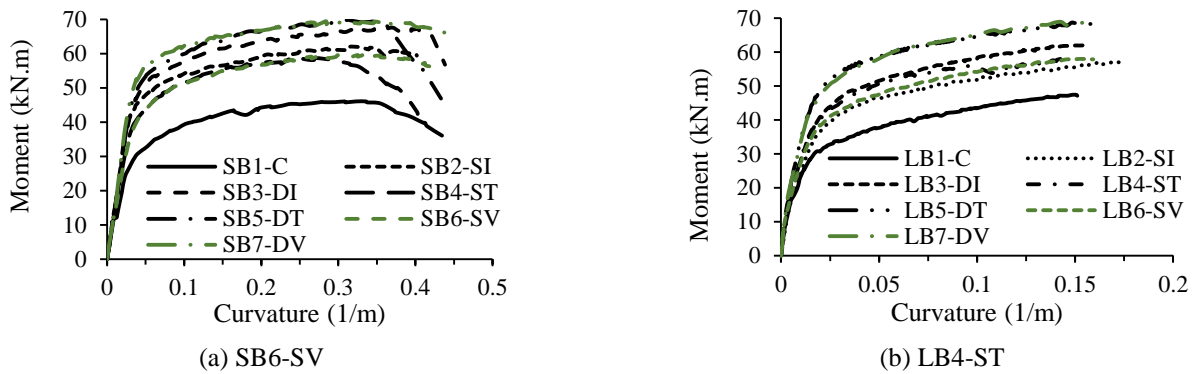


Fig. 9 Moment vs mid-span curvature relationships

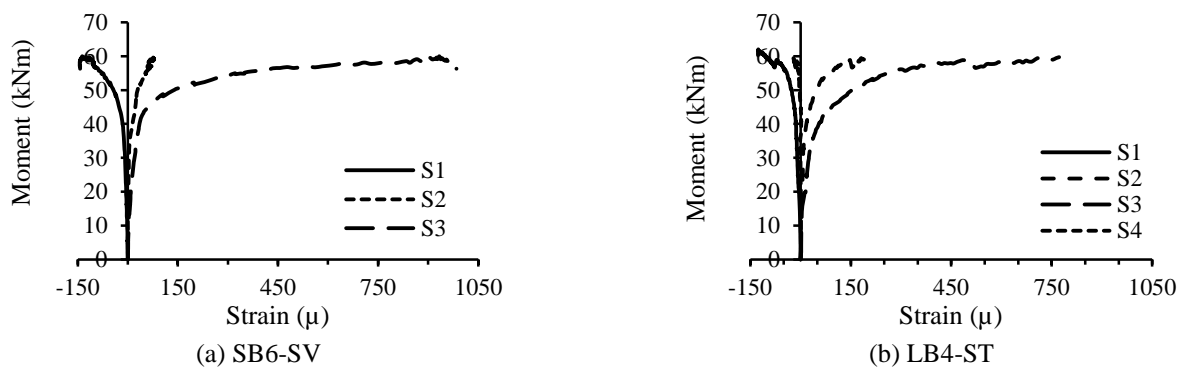


Fig. 10 Moment vs strain relationships

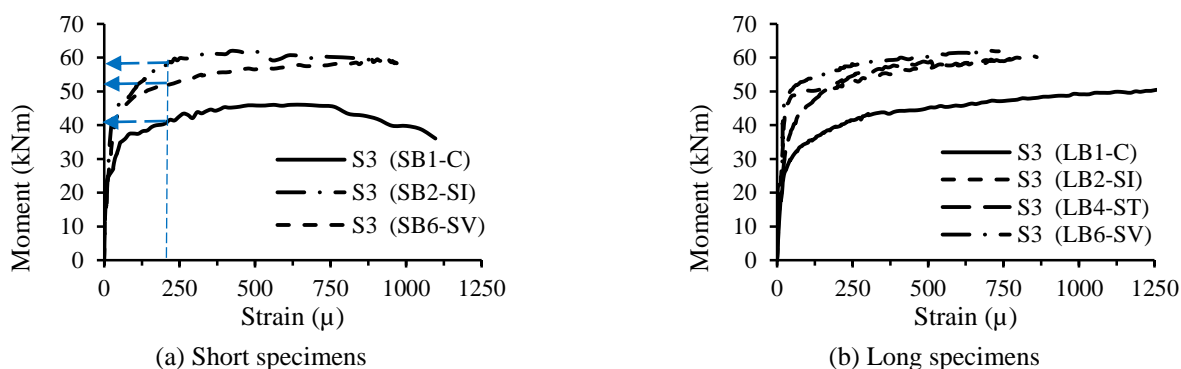


Fig. 11 Comparison of the tensile strain at the bottom flange of tested specimens

Table 3 Summary of the test results of CFST specimens

Specimens designation	M_u (kN.m)	MIP (+%)	E.A (kN.m)	K_i (kN. m ²)	K_s (kN. m ²)	M_{u-FE} (kN.m)	M_{u-FE}/M_u
LB1-C	46.0	-	6.2	2,222	1,966	-	-
LB2-SI	54.4	18.2	7.3	3,033	2,797	-	-
LB3-DI	60.4	31.2	8.2	3,519	2,854	-	-
LB4-ST	56.5	22.7	8.0	3,076	2,681	-	-
LB5-DT	66.9	45.4	9.4	3,675	3,187	-	-
LB6-SV	56.3	22.4	7.5	3,149	2,856	-	-
LB7-DV	67.9	47.6	9.3	3,739	3,119	-	-
SB1-C	45.9	-	6.3	2,511	2,315	45.8	0.998
SB2-SI	60.7	32.3	7.9	3,655	3,427	60.1	0.989
SB3-DI	65.2	42.1	8.7	3,866	3,603	65.5	1.004
SB4-ST	58.7	27.9	8.3	3,036	2,817	59.5	1.013
SB5-DT	68.3	48.8	9.4	4,065	3,665	69.7	1.020
SB6-SV	59.3	29.1	7.7	3,241	2,899	60.2	1.016
SB7-DV	69.0	50.2	9.4	4,002	3,437	71.1	1.031
MV							1.010
COV							0.013

Table 4 Verification of the experimental M_u values with the predicted values from existing standards

Specimens designation	M_u (kN.m)	M_{u-EC4} (kN.m)	M_{u-EC4}/M_u	M_{u-Han} (kN.m)	M_{u-Han}/M_u
LB1-C	45.9	34.8	0.759	39.2	0.852
LB2-SI	60.7	35.1	0.578	39.2	0.721
LB3-DI	65.2	35.4	0.542	39.2	0.650
LB4-ST	58.7	35.3	0.601	39.2	0.694
LB5-DT	68.3	35.7	0.522	39.2	0.586
LB6-SV	59.3	35.3	0.595	39.2	0.696
LB7-DV	69.0	35.7	0.518	39.2	0.577
SB1-C	46.0	34.8	0.757	39.2	0.854
SB2-SI	54.4	35.1	0.645	39.2	0.646
SB3-DI	60.4	35.4	0.586	39.2	0.601
SB4-ST	56.5	35.3	0.625	39.2	0.668
SB5-DT	66.9	35.7	0.533	39.2	0.574
SB6-SV	56.3	35.3	0.626	39.2	0.662
SB7-DV	67.9	35.7	0.525	39.2	0.569
MV			0.604	0.670	
COV			0.126	0.132	

$$M_{u-Han} = \gamma_m W_{scm} f_{scy} \quad (7)$$

$$\gamma_m = 1.04 + 0.48 \ln(\xi + 0.1) \quad (8)$$

$$f_{scy} = (1.18 + 0.85 \xi) f_{ck} \quad (9)$$

$$\xi = (A_s f_y) / (A_c f_{ck}) \quad (10)$$

$$W_{scm} = D^3 / 6 \quad (11)$$

where W_{scm} is the section modulus for the rectangular/square sections of the steel tube. The f_{scy} , A_s , A_c and γ_m are yield strength of the composite section, cross-section area of steel tube, the cross-section area of concrete core and flexural strength index, respectively. The f_{ck} is the characteristic concrete strength which is equal to $0.67f_{cu}$, where, f_{cu} is the characteristic concrete cube strength at 28-days. Lastly, the ξ is the confinement factor which describes the composite action between the materials of steel tube and concrete core as per the unified theory (Han *et al.* 2001).

Table 4 shows the comparison between the M_u values obtained from the current experimental tests and the ones theoretically predicted from the mentioned standards. The mean value (MV) predicted from the ratio of M_{u-EC4}/M_u are about 0.604, with a coefficient of variation (COV) of 0.126. The formula of Han (2004) has achieved a slightly better prediction of the M_u values of the experimental results than the EC4, in which the MV and COV are equal to 0.670 and 0.132, respectively. Generally, in this comparison study, the lower prediction by the methods of EC4 and Han compared to the current experimental results occurred because both of these theoretical methods do not consider the effects of the additional steel stiffeners that were provided inside the CFST beams, where the effects of the steel section are usually estimated in these methods from the dimensions of the tube (D and t) only, see the Eqs. 1 - 11. Therefore, a new formula needs to be established to adequately predict the moment capacity of the stiffened CFST beams with internal steel stiffeners.

3.4 Flexural stiffness

The flexural stiffness performance of the stiffened CFST beams is discussed in this section. As explained earlier, at the initial loading stage, all of the tested specimens behaved in an elastic manner, followed by an inelastic behaviour in the remaining loading stages. According to the moment vs curvature relationships, the flexural stiffness at the initial level (K_i) and the serviceability level (K_s) were estimated at the moment values of $0.2M_u$ and $0.6M_u$, respectively (Han *et al.* 2006b, Al Zand *et al.* 2016). The K_i and K_s values obtained from the tested CFST specimens are estimated and presented earlier in Table 3. Generally, the specimens with a shorter span exhibited a slightly stiffer behaviour than those the ones with a longer span. The flexural stiffness

values have gradually improved as the specimen's cross-section moment of inertia for the steel increased. Thus, the specimens with double stiffeners had higher values than the corresponding specimens. For example, as given in Table 3, the obtained K_i value of SB1-C was about 2,511 kN.m², which had increased to 3,655 kN.m² (+45.5%) when a single I-shaped stiffener was employed (SB2-SI). The value had further increased to 3,866 kN.m² (+53.9%) when double stiffeners of the same shape were incorporated (SB3-DI). For all tested specimens, the flexural stiffeners at the serviceability level (K_s) have exhibited lower values than the corresponding K_i values with ratios of about 0.81-0.92.

Four (4) theoretical standards are used to evaluate the flexural stiffness values (K_i and K_s) that were obtained from the current experimental study, namely, BS5400 (2005), EC4 (2004), AISC (2010), and AIJ (1997). The details of these theoretical formulae are as follows

$$K = F_1 E_s I_s + F_2 E_c I_c \quad (12)$$

where the F_1 is the reduction factor for the steel stiffness part, which is equal to 0.95 in the standard BS5400 and equal to 1.0 for the other standards. The F_2 is the reduction factor for the concrete stiffness part, which is equal to 0.45, 0.2 and 0.6 in the standards BS5400, AIJ and EC4, respectively. Meanwhile, in standard AISC (2010), the F_2 value is varied ($F_2 = 0.6 + 0.2 (A_s / (A_s + A_c)) \leq 0.9$). For all standards, the I_s and I_c are the cross-section moment of inertia for the steel and concrete, respectively. E_s and E_c are the moduli of elasticity for the steel tube and concrete material. The value of E_c are estimated for each standard separately, which is equal to $[450 f_{cu}]$, $[9500.(f_{ck}+8)^{1/3}]$, $[4733.(f_c)^{1/2}]$, and $[4733.(f_c / 19.6)^{1/2}]$ for the standards BS5400, EC4, AISC-2010 and AIJ-1997, respectively. f_c is the characteristic concrete cylinder strength at 28-days. An additional theoretical model to predict the flexural stiffness K_i and K_s values that was presented in (Han *et al.* 2006b) was used in this comparison study, which is expressed as follows

$$K_{i-Han} = 0.2M_u / \phi_i \quad (13)$$

$$\phi_i = [(10.64B_c + 91.18) + (8.66B_c + 5.93)\xi] B_s^{0.82} / (E_s D) \quad (14)$$

$$K_{s-Han} = 0.6M_u / \phi_s \quad (15)$$

$$\phi_s = [(38.9B_c + 319.11) + (12.61B_c + 23.1)\xi] B_s^{0.82} / (E_s D) \quad (16)$$

where, the β_s and β_c are equal to $f_y/345$ and $f_{cu}/30$, respectively.

For the initial flexural stiffness (K_i), EC4 and AISC have overestimated the values compared to the experimental results, with MVs equal to 1.296 and 1.293 with COVs of 0.144 and 0.134, respectively, as presented in Table 5. The same standards EC4 and AISC have further overestimated the experimental stiffness values at the serviceability-level (K_s), with MVs of 1.457 and 1.453,

respectively. This is because of the decrease in the effective stiffness value at the serviceability-level ($0.6M_u$) was not considered by these standards in their formulas. However, compared to the experimental results, the BS5400 and AIJ standards have underestimated the experimental K_i values, with MVs of 0.855 and 0.778 and COVs of 0.128 and 0.117, respectively. This is due to both the BS5400 and AIJ are using lower reduction factors for the concrete stiffness part compared with the other standards, which are equal to 0.45 and 0.2, respectively. In the other hand, Han *et al.* (2006b) consider the change in the flexural stiffness behaviour from the initial level to the serviceability level; thus, compared to the corresponding experimental results, their formula has accomplished the best prediction values. The MVs from K_{i-Han}/K_i and K_{s-Han}/K_s are about 0.911 and 0.892, respectively, with sufficient COVs which are equal to 0.058 and 0.072.

3.5 Energy absorption

The energy absorption (EA) index of each tested CFST specimen was calculated from the area under its load-deflection curve (Al Zand *et al.* 2016, Javed *et al.* 2018), in which the area is estimated up to the deflection limits corresponding to the M_u value. This index is used to evaluate the structural member performance under seismic loading, and a member that has a higher EA index demonstrates superior performance during an earthquake (Javed *et al.* 2018). Table 3 shows the estimated EA indices of the tested specimens. According to the total area under the load-deflection curves, the stiffened CFST specimens with double stiffeners have achieved higher EA values than the other corresponding specimens. This is expected since these specimens (with double stiffeners) have the highest load capacities. For example, the EA of specimen SB1-C is equal to 6.3 kN.m; this value had approximately increased with a range of about 23% to 32% when a single stiffener was incorporated into specimens SB2-SI, SB4-ST, and SB6-SV. Then, this improvement further increased with a range of about 39% to 50% when double stiffeners were incorporated. Similar performance was recorded for the longer specimens but with slight differences in their EA values.

4. Finite element analysis

4.1 Description of the FE modelling

Finite element (FE) models were developed and analysed using the nonlinear software (ABAQUS) to simulate the suggested stiffened CFST specimens. The boundary conditions for the typical 3-D quarter FE model are shown in Fig. 12 for model SB7-DV as an example. An incremental displacement was assigned at the positions of point loads to represent the actual applied loads. In general, each model has two material components (steel and concrete). The element type C3D8R was chosen for the steel and concrete components; a solid element with 8-node linear brick-reduced integration with 6-degrees of freedom

for each node.

The value of friction coefficient between the steel tube and the concrete core could be affected by several parameters, such as the dimensions of the tube, cross-section shape, loading type/rate and type of concrete (Al Zand *et al.* 2018; Moon *et al.* 2012; Javed *et al.* 2017). Thus, after conducting several preliminary FE analyses in the current study, a friction coefficient was taken as 0.5 with “Hard” contact pressure to characterise the mechanical contact between the inner surface of the steel tube and the outer surface of the concrete core. However, in the current FE analysis, a full tie interaction was suggested to represent the mechanical contact between the surfaces of the internal steel stiffeners and the concrete, since no-slip failure was observed in the experimental tests (as discussed earlier in Section 3.1).

The steel tube and steel stiffeners are considered isotropic material in the FE modelling. Thus, the modulus of elasticity (E_s) and the Poisson's ratio of a steel material were identified in the elastic-isotropic section, and the plastic-isotropic section was used to identify the steel yield strength and the related strain values. The concrete was also considered an isotropic material at the elastic stage, while, at the inelastic stage, it is capable of crushing at the compression stress and cracking at the tension stress (Al Zand *et al.* 2018). Thus, the compressive and tensile strengths vs strain relationships of the concrete were identified in the damaged plasticity section, while, the section of elastic-isotropic was used to identify the modulus of elasticity (E_c). Generally, the current study has used the same modelling concept and constitutive stress-strain relationships of the steel and concrete materials of Al Zand *et al.* (2018), as presented in Fig. 13.

4.2 Verification of the FE models

The same properties and boundary conditions of the experimental CFST specimens were used to develop seven (7) FE models. The aim is to simulate the flexural performance of the stiffened CFST specimens with a short span since both of the short and long specimens were achieved close results of bending capacities (as highlighted earlier in Section 3.3). The M_{u-FE} values obtained from the analyses of these seven (7) models have marginally overestimated the experimental M_u values of the corresponding specimens, as compared in Table 3. The MV predicted from the ratio of M_{u-FE}/M_u is about 1.010 with COV equal to 0.013, which is sufficient estimation.

A convergence study was conducted for the developed FE models in order to achieve accurate results through selecting the significant meshing size (number of elements). As an example, the convergence study for the bending capacity of model SB2-SI presented in Fig. 14.

The flexural performance of the developed FE CFST models have fairly simulated the experimental performance, and the comparison between their moment-deflection curves are shown in Fig. 15. Furthermore, the typical tube buckling failure obtained from the FE analysis at the ultimate loading stage (M_u) is presented in Fig. 16. These sections are taken at the position located between the point

Table 5 Verification of the experimental K_i and K_s values with the predicted values from existing standards

Specimens designation	K_{BS} / K_i	K_{BS} / K_s	K_{EC4} / K_i	K_{EC4} / K_s	K_{AISC} / K_i	K_{AISC} / K_s	K_{AIJ} / K_i	K_{AIJ} / K_s	K_{i_Han} / K_i	K_{s_Han} / K_s
LB1-C	1.143	1.292	1.782	2.013	1.746	1.973	1.016	1.148	1.049	1.032
LB2-SI	0.879	0.953	1.349	1.463	1.336	1.449	0.791	0.858	0.908	0.858
LB3-DI	0.805	0.993	1.213	1.496	1.214	1.497	0.736	0.908	0.869	0.932
LB4-ST	0.889	1.020	1.353	1.553	1.350	1.548	0.805	0.924	0.930	0.929
LB5-DT	0.816	0.941	1.209	1.394	1.223	1.411	0.756	0.872	0.922	0.926
LB6-SV	0.882	0.972	1.336	1.473	1.333	1.470	0.802	0.884	0.906	0.870
LB7-DV	0.824	0.988	1.212	1.453	1.227	1.471	0.769	0.922	0.920	0.960
SB1-C	1.012	1.097	1.577	1.710	1.545	1.676	0.899	0.975	0.926	0.874
SB2-SI	0.729	0.778	1.119	1.194	1.109	1.183	0.656	0.700	0.842	0.781
SB3-DI	0.733	0.786	1.104	1.185	1.105	1.186	0.670	0.719	0.855	0.798
SB4-ST	0.900	0.970	1.371	1.478	1.367	1.474	0.816	0.879	0.979	0.919
SB5-DT	0.737	0.818	1.093	1.212	1.106	1.227	0.683	0.758	0.851	0.822
SB6-SV	0.856	0.957	1.298	1.451	1.295	1.447	0.779	0.871	0.926	0.901
SB7-DV	0.770	0.897	1.133	1.318	1.146	1.334	0.718	0.836	0.873	0.884
MV	0.855	0.962	1.296	1.457	1.293	1.453	0.778	0.875	0.911	0.892
COV	0.128	0.131	0.144	0.143	0.134	0.136	0.117	0.122	0.058	0.072

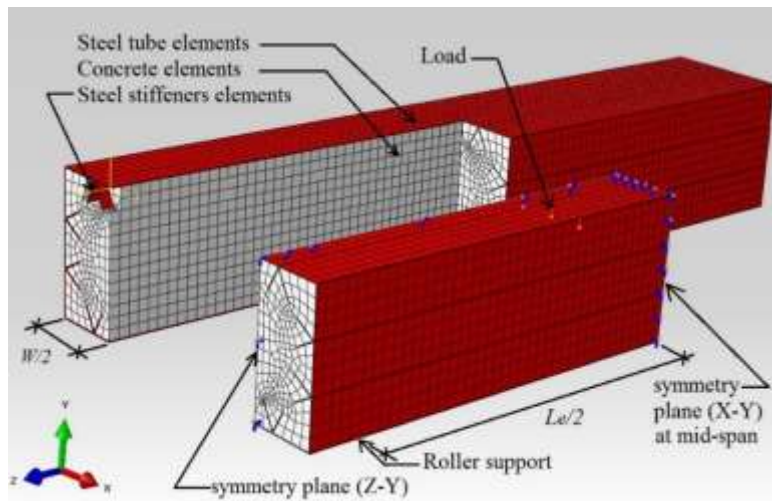


Fig. 12 Typical 3-D quarter FE model – SB7-DV.

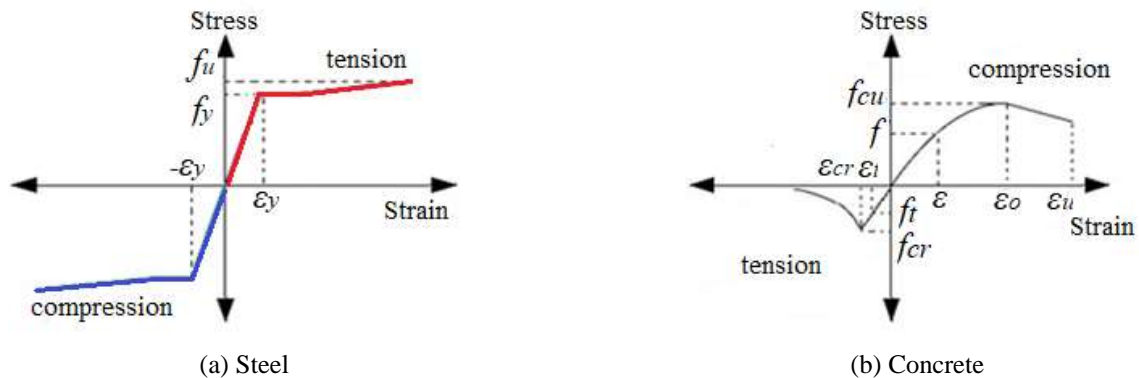


Fig. 13 Constitutive materials stress-strain relationships (Al Zand *et al.* 2018).

load ($L_e/3$) and mid-span ($L_e/2$) of the model, confirming that the current FE analyses can fairly represent the actual tube's failure occurred for the tested CFST specimens (which are earlier shown in Figs. 4-6).

4.3 Effects of internal steel stiffeners thickness

The effects of varied parameters such as the infill concrete strengths, steel yielding strengths and steel tube thickness on the performance of the square CFST beams were investigated earlier in several studies (Han *et al.* 2006b; Jiang *et al.* 2013; Javed *et al.* 2017). Therefore, in the current numerical analyses, the influence of using the varied thickness of the internal stiffeners (t_{st}) on the flexural performance of the suggested stiffened CFST beams was investigated. Two additional thicknesses of stiffener were adopted in this study (3.0 mm and 4.5 mm). The boundary conditions and the rest of the material properties remained the same as described earlier for the experimental specimens.

From the FE analyses, the moment capacity of the stiffened models has improved due to increasing their stiffener's thickness, as summarised in Fig. 17. This performance can be considered logical since the overall steel tube cross-section area (A_s) has increased due to the increases of internal stiffeners' thickness. Thus, the FE models with double stiffeners achieved higher loading improvements compared to the corresponding models with a single stiffener that have the same stiffeners' thickness. For example, the M_{u-FE} value of model SB4-ST with 1.5 mm stiffener's thickness was equal to 59.5 kN.m. This value had increased by about 18% (70.3 kN.m) and 33% (78.8 kN.m) when the thickness of their internal stiffeners (t_{st}) increased to 3.0 mm and 4.5 mm, respectively. For the same stiffeners shape, in the case of using double stiffeners (SB5-DT), the percentages of bending capacities were further increased to 27% (88.3 kN.m) and 48% (103.1 kN.m) when used stiffeners with 3.0 mm and 4.5 mm thickness, respectively, compared to the same model with 1.5 mm stiffener's thickness. In general, similar behaviour was observed for the other stiffened FE models but with different percentages of improvements.

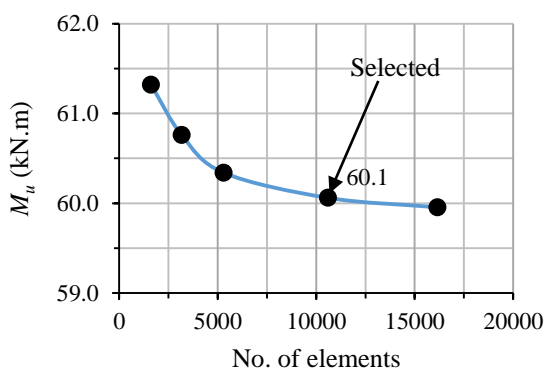


Fig. 14 Convergence study for the FE model (SB2-SI)

However, increasing the thickness of the stiffener does not influence the tube local buckling failure which was remained without change ($t=1.5$ mm).

5. Conclusions

The conclusions of the current study are summarised as follows:

- The internal steel stiffeners have delayed and mitigated the tube's outward local buckling failure, which usually occurs at the top half of the cross-section of the simply supported CFST beam due to the high compression stress. Increasing the number of stiffeners is more effective in restricting the tube's local buckling compared to the effect of increasing their thickness.

- In addition, the steel tube cross-sectional area has increased due to the introduction of the internal steel stiffeners, particularly at the top and bottom steel flange; thus, the moment capacity of the stiffened slender cold-formed CFST specimen has substantially improved with either the increasing number of stiffeners or their thickness. For example, providing a single T-shaped stiffener at each side of the tube has enhanced the moment capacity of the slender CFST beam by about 27.9% compared to the unstiffened specimen; this percentage had further improved to 48.8% when double stiffeners were used with the same shape.

- The flexural stiffness of the stiffened CFST specimens has gradually enhanced due to the presence of the internal stiffeners since they have increased the moment of inertia for the steel part. Compared to the unstiffened specimen, the initial stiffness of the specimen that was stiffened with a single V-shape stiffener had increased by 29.0%, and by 59.3% when double V-shaped stiffeners were used, as an example.

- The capability of the slender CFST specimen to absorb energy is improved substantially by the incorporation of internal stiffeners. The EA value of the control specimen has increased by about 22.6% and 50.3% when internally stiffened with single and double V-shaped stiffeners, respectively.

- The moment capacity and the failure modes of the stiffened CFST beams have been successfully predicted by the FE models. The FEM models will be used for further numerical investigation of the stiffened CFST beams.

- The results obtained from the experimental tests and the numerical analyses compared well to the corresponding theoretical values predicted from various existing standards, namely, EC4, AISC, BS5400, and AIJ, and other methods.

As the influence of adopting the internal steel stiffeners in improving the behaviour of the slender CFST beams has been demonstrated in the current research, further experimental and numerical investigations are required to develop a new theoretical formula that will enable the prediction of the moment capacity of the stiffened CFST beams with steel stiffeners. Furthermore, in the case of slender CFST beams subjected to static flexural loading, it

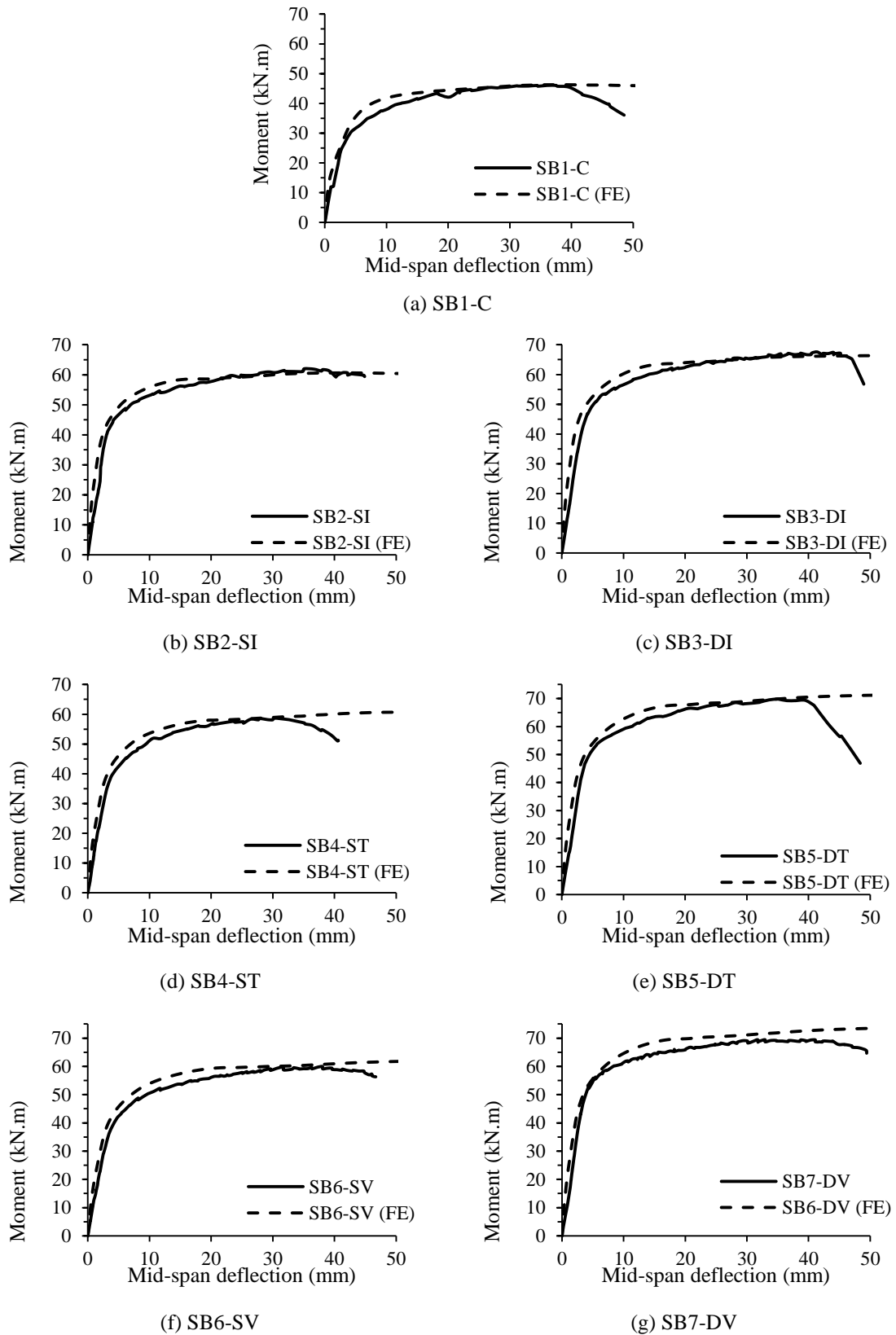


Fig. 15 Verification of the moment-deflection relationships of the FE models

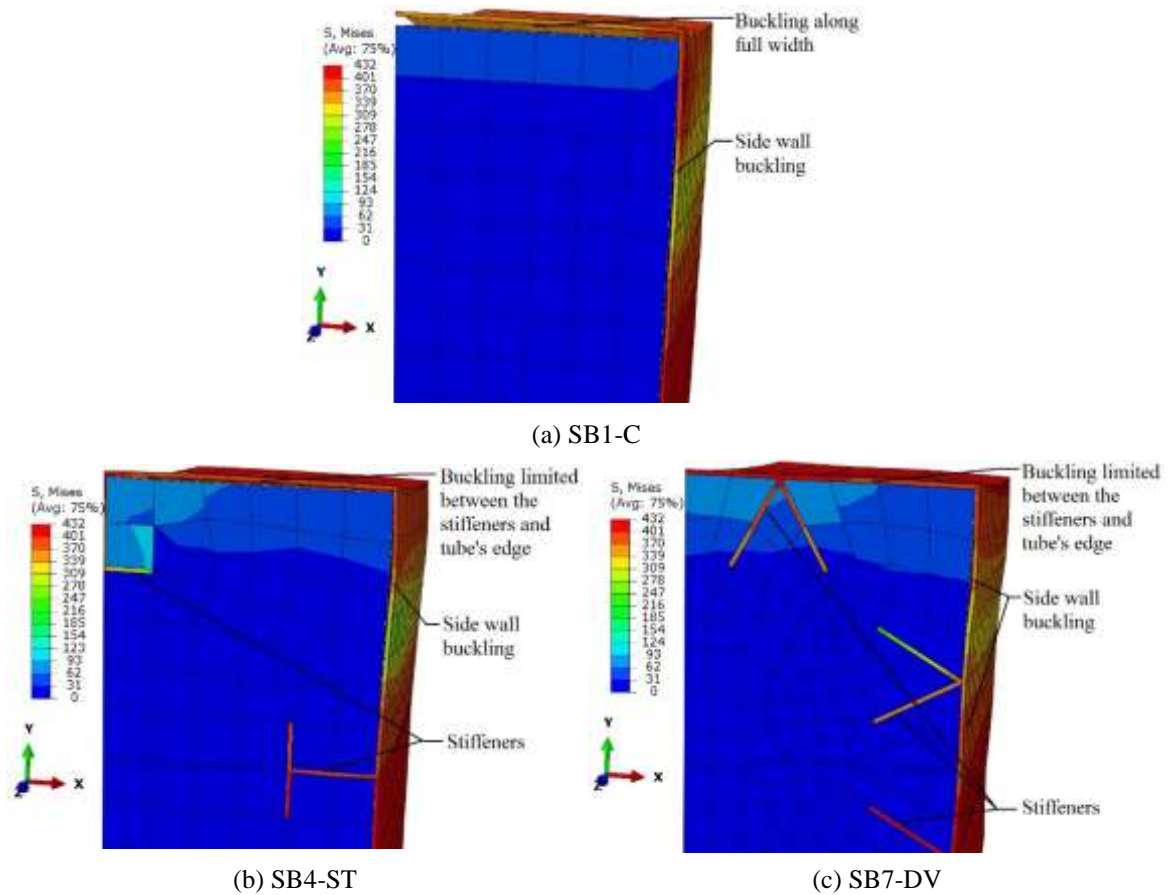


Fig. 16 Typical buckling failures for the stiffened FE CFST model (all units in MPa)

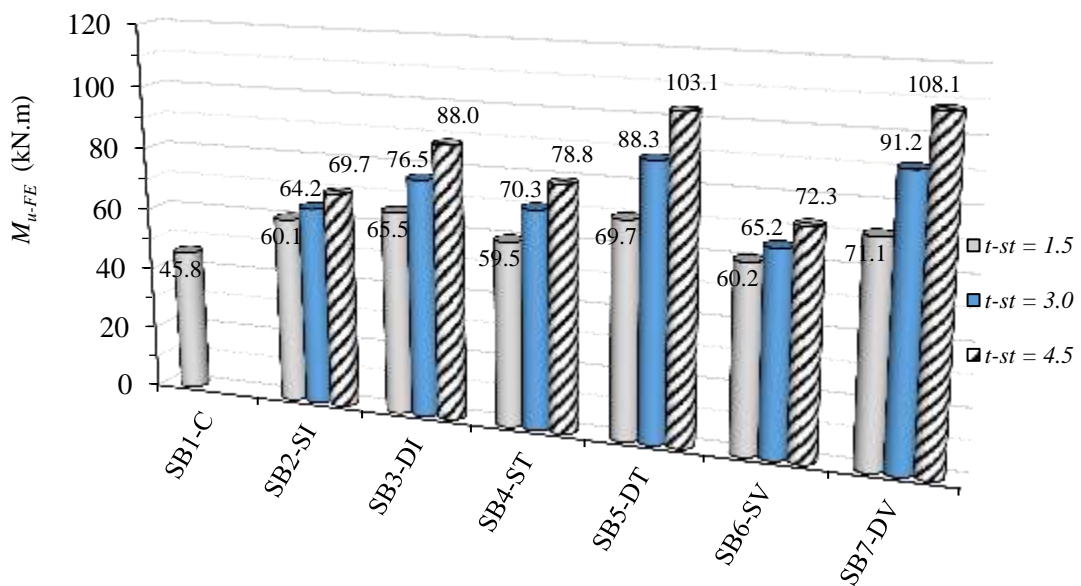


Fig. 17 Comparison between the predicted M_{u-FE} values – varied stiffener thickness

is suggested that to reduce the stiffening cost, internal steel stiffeners along the sides and lengths are to be provided only in areas subjected to the high compression stress, which is required to prevent/delay the tubes outward local buckling.

Acknowledgments

The authors gratefully acknowledge the financial support for the postdoctoral research provided by Universiti Kebangsaan Malaysia (UKM) with project code No. (MI-2018-010).

References

- Abdalla, S., Abed, F. and AlHamaydeh, M. (2013), "Behavior of CFSTs and CCFSTs under quasi-static axial compression", *J. Constr. Steel Res.*, **90**, 235-244. <https://doi.org/10.1016/j.jcsr.2013.08.007>
- AIJ (1997), Recommendations for Design and Construction of Concrete Filled Steel Tubular Structures, Architectural Institute of Japan (AIJ).
- AISC-LRFD (1999), Load and resistance factor design specification for structural steel buildings. Chicago: American Institute of Steel Construction (AISC), Inc.,
- AISC (2010), Specification for structural steel buildings. American Institute of Steel Construction (AISC), Chicago, IL;
- AL-Shaar, A.A. and Göğüş, M.T. (2018), "Performance of retrofitted self-compacting concrete-filled steel tube beams using external steel plates", *Adv. Mater. Sci. Eng.*, **2018**, Article ID 3284745, 18 pages. <https://doi.org/10.1155/2018/3284745>.
- Al-Zand, A.W., Hosseinpour, E. and Tawfeeq, W.M. (2017), "The effects of filling the rectangular hollow steel tube beam with concrete: an experimental case study", *J. Civil Eng. Researchers.* **1**(3), 23-30. <http://www.journals-searchers.com/ojs/index.php/jcer/article/view/22>.
- Al Zand, A.W., Badaruzzaman, W.H.W., Mutalib, A.A. and Hilo, S.J. (2016), "The enhanced performance of CFST beams using different strengthening schemes involving unidirectional CFRP sheets: An experimental study", *Eng. Struct.*, **128** 184-198. <https://doi.org/10.1016/j.engstruct.2016.09.044>
- Al Zand, A.W., Badaruzzaman, W.H.W., Mutalib, A.A. and Hilo, S.J. (2018), "Flexural behavior of CFST beams partially strengthened with unidirectional CFRP sheets: experimental and theoretical study", *J. Compos. Constr.*, **22**(4), 04018018. [https://doi.org/10.1061/\(ASCE\)CC.1943-5614.0000852](https://doi.org/10.1061/(ASCE)CC.1943-5614.0000852).
- Al Zand, A.W., Hosseinpour, E. and Badaruzzaman, W.H.W. (2018), "The influence of strengthening the hollow steel tube and CFST beams using U-shaped CFRP wrapping scheme", *Struct. Eng. Mech.*, **66**(2), 229-235. <https://doi.org/10.12989/sem.2018.66.2.229>.
- AS 4100 (1998), Standards Association of Australia. Steel structures code. Sydney, Australia.
- Bahrami, A., Badaruzzaman, W.H.W. and Osman, S.A. (2011), "Nonlinear analysis of concrete-filled steel composite columns subjected axial to loading", *Struct. Eng. Mech.*, **39**(3), 383-398. <http://dx.doi.org/10.12989/sem.2011.39.3.383>.
- Bahrami, A., Badaruzzaman, W.H.W. and Osman, S.A. (2012), "Structural behaviour of tapered concrete-filled steel composite (TCFSC) columns subjected to eccentric loading", *Comput. Concrete*, **9**(6), 403-426. <http://dx.doi.org/10.12989/cac.2012.9.6.403>.
- Bahrami, A., Badaruzzaman, W.H.W. and Osman, S.A. (2013), "Behaviour of stiffened concrete-filled steel composite (CFSC) stub columns", *Latin Am. J. Solids Struct.*, **10**(2), 409-440. <http://dx.doi.org/10.1590/S1679-78252013000200009>.
- Bahrami, A., Badaruzzaman, W.H.W. and Osman, S.A., (2014). "Numerical study of concrete-filled steel composite (CFSC) stub columns with steel stiffeners". *Latin Am. J. Solids Struct.*, **11**(4), 683-703. <http://dx.doi.org/10.1590/S1679-78252014000400008>.
- BS5400 (2005), Steel, Concrete and Composite Bridges. Part 5: code of practice for the design of composite bridges. British Standards Institution, London (UK).
- Chen, J. and Jin, W.I. (2010), "Experimental investigation of thin-walled complex section concrete-filled steel stub columns", *Thin-Wall. Struct.*, **48**(9), 718-724. <https://doi.org/10.1016/j.tws.2010.05.001>.
- Chen, J., Liu, X., Liu, H. and Zeng, L. (2018), "Axial compression behavior of circular recycled concrete-filled steel tubular short columns reinforced by silica fume and steel fiber", *Steel Compos. Struct.*, **27**(2), 193-200. <http://dx.doi.org/10.12989/scs.2018.27.2.193>.
- EC4 (2004), European Committee for Standardization. Design of Composite Steel and Concrete Structures – Part 1.1: General rules and rules for buildings, European Committee for Standardization (Eurocode 4), Brussels; Belgium.
- EC3 (2002), European Committee for Standardization. Design of Steel Structures- Part 1.1, General rules and rules for buildings. European Committee for Standardization (Eurocode 3), Brussels; Belgium.
- Ekmekyapar, T. and Al-Eliwi, B.J. (2017), "Concrete filled double circular steel tube (CFDCST) stub columns", *Eng. Struct.*, **135** 68-80. <https://doi.org/10.1016/j.engstruct.2016.12.061>.
- Hosseinpour, E., Baharom, S., Badaruzzaman, W.H.W., Shariati, M. and Jalali, A., (2018). "Direct shear behavior of concrete filled hollow steel tube shear connector for slim-floor steel beams", *Steel Compos. Struct.*, **26**(4), 485-499. <https://doi.org/10.12989/scs.2018.26.4.485>
- Guler, S., Copur, A. and Aydogan, M. (2012), "Flexural behaviour of square UHPC-filled hollow steel section beams", *Struct. Eng. Mech.*, **43**(2), 225-237. <http://dx.doi.org/10.12989/sem.2012.43.2.225>.
- Han, L.H., Zhao, X.L. and Tao, Z. (2001), "Tests and mechanics model for concrete-filled SHS stub columns, columns and beam-columns", *Steel Compos. Struct.*, **1**(1), 51-74. <http://dx.doi.org/10.12989/scs.2001.1.1.051>.
- Han, L.H. (2004), "Flexural behaviour of concrete-filled steel tubes", *J. Constr. Steel Res.*, **60**(2), 313-337. <https://doi.org/10.1016/j.jcsr.2003.08.009>.
- Han, L.H., Huang, H., Tao, Z. and Zhao, X.L. (2006a), "Concrete-filled double skin steel tubular (CFDST) beam-columns subjected to cyclic bending", *Eng. Struct.*, **28**(12), 1698-1714. <https://doi.org/10.1016/j.engstruct.2006.03.004>.
- Han, L.H., Lu, H., Yao, G.H. and Liao, F.Y. (2006b), "Further study on the flexural behaviour of concrete-filled steel tubes", *J. Constr. Steel Res.*, **62**(6), 554-565. <https://doi.org/10.1016/j.jcsr.2005.09.002>.
- Han, L.H., Li, W. and BJORHOVDE, R. (2014), "Developments and advanced applications of concrete-filled steel tubular (CFST) structures: Members", *J. Constr. Steel Res.*, **100**, 211-228. <https://doi.org/10.1016/j.jcsr.2014.04.016>.
- Hassan, M.M., Mahmoud, A.A. and Serror, M.H. (2016), "Behavior of concrete-filled double skin steel tube beam-columns", *Steel Compos. Struct.*, **22**(5), 1141-1162. <http://dx.doi.org/10.12989/scs.2016.22.5.1141>.
- Helena, H.J. and Knight, G. (2005), "Behaviour of cold-formed steel hollow and concrete-filled members", *Steel Compos.*

- Struct.*, **5**(1), 35-47. <http://dx.doi.org/10.12989/scs.2005.5.1.035>.
- Hilo, S.J., Badaruzzaman, W.H.W., Osman, S.A. and Al Zand, A.W. (2015), "Axial load behavior of a composite wall strengthened with an embedded octagon cold-formed steel", *Appl. Mech. Mater.*, **754**, 437-441. <https://doi.org/10.4028/www.scientific.net/AMM.754-755.437>.
- Huang, C., Yeh, Y.K., Liu, G.Y., Hu, H.T., Tsai, K., Weng, Y., Wang, S. and Wu, M.H. (2002), "Axial load behavior of stiffened concrete-filled steel columns", *J. Struct. Eng.*, **128**(9), 1222-1230. [10.1061/~ASCE:10733-9445~2002:128:9~1222!](https://doi.org/10.1061/~ASCE:10733-9445~2002:128:9~1222!).
- Javed, M.F., Sulong, N.R., Memon, S.A., Rehman, S.K.U. and Khan, N.B. (2018), "Flexural behaviour of steel hollow sections filled with concrete that contains OPBC as coarse aggregate", *J. Constr. Steel Res.*, **148**, 287-294. <https://doi.org/10.1016/j.jcsr.2018.05.035>.
- Javed, M.F., Sulong, N.R., Memon, S.A., Rehman, S.K.U. and Khan, N.B. (2017), "FE modelling of the flexural behaviour of square and rectangular steel tubes filled with normal and high strength concrete", *Thin-Wall. Struct.*, **119**, 470-481. <https://doi.org/10.1016/j.tws.2017.06.025>.
- Jiang, A.Y., Chen, J. and Jin, W.I. (2013), "Experimental investigation and design of thin-walled concrete-filled steel tubes subject to bending", *Thin-Wall. Struct.*, **63**, 44-50. <https://doi.org/10.1016/j.tws.2012.10.008>.
- Kang, J.Y., Choi, E.S., Chin, W.J. and Lee, J.W. (2007), "Flexural behavior of concrete-filled steel tube members and its application", *Int. J. Steel Struct.*, **7**(4), 319-324.
- Lee, S., Kim, S., Bang, J., Won, Y. and Choi, S. (2011), "Structural characteristics of welded built-up square concrete filled tubular stub columns associated with concrete strength", *Procedia Eng.*, **14**, 1140-1148. <https://doi.org/10.1016/j.proeng.2011.07.143>.
- Liang, W., Dong, J. and Wang, Q. (2018), "Axial compressive behavior of concrete-filled steel tube columns with stiffeners", *Steel Compos. Struct.*, **29**(2), 151-159. <http://dx.doi.org/10.12989/scs.2018.29.2.151>.
- Ling, Y., Feng, W., Zhao, J. and Li, Y. (2014), "Study on the ultimate bearing capacity of concrete filled steel square tubular short column with PBL", *Adv. Mater. Res.*, **941-944**, 770-775. <https://doi.org/10.4028/www.scientific.net/AMR.941-944.770>.
- Lu, Y., Liu, Z., Li, S. and Hu, J. (2018), "Axial compression behavior of hybrid fiber reinforced concrete filled steel tube stub column", *Constr. Build. Mater.*, **174**, 96-107. <https://doi.org/10.1016/j.conbuildmat.2018.04.089>.
- Lu, Y., Liu, Z., Li, S. and Li, N. (2018), "Bond behavior of steel fibers reinforced self-stressing and self-compacting concrete filled steel tube columns", *Constr. Build. Mater.*, **158**, 894-909. <https://doi.org/10.1016/j.conbuildmat.2017.10.085>.
- Lu, Y., Liu, Z., Li, S. and Li, W. (2017), "Behavior of steel fibers reinforced self-stressing and self-compacting concrete-filled steel tube subjected to bending", *Constr. Build. Mater.*, **156**, 639-651. <https://doi.org/10.1016/j.conbuildmat.2017.09.019>.
- Qian, J., Zhang, Y., Ji, X. and Cao, W. (2011), "Test and analysis of axial compressive behavior of short composite-sectioned high strength concrete filled steel tubular columns", *Jianzhu Jiegou Xuebao (Journal of Building Structures)*, **32**(12), 162-169. http://en.cnki.com.cn/Article_en/CJFDTotl-JZJB201112019.htm.
- Moon, J., Roeder, C.W., Lehman, D.E. and Lee, H.E. (2012), "Analytical modeling of bending of circular concrete-filled steel tubes", *Eng. Struct.*, **42**, 349-361. <https://doi.org/10.1016/j.engstruct.2012.04.028>.
- Song, Y., Li, J. and Chen, Y. (2019), "Local and post-local buckling of normal/high strength steel sections with concrete infill", *Thin-Wall. Struct.*, **138**, 155-169. <https://doi.org/10.1016/j.tws.2019.02.004>.
- Sundarraja, M.C. and Prabhu, G.G. (2013), "Flexural behaviour of CFST members strengthened using CFRP composites", *Steel Compos. Struct.*, **15**(6), 623-643. <http://dx.doi.org/10.12989/scs.2013.15.6.623>.
- Tao, Z., Han, L.H. and Wang, D.Y., (2007). "Experimental behaviour of concrete-filled stiffened thin-walled steel tubular columns", *Thin-Wall. Struct.*, **45**(5), 517-527. <https://doi.org/10.1016/j.tws.2007.04.003>.
- Wang, R., Han, L.H., Nie, J. G. and Zhao, X.L. (2014), "Flexural performance of rectangular CFST members", *Thin-Walled Struct.*, **79**, 154-165. <https://doi.org/10.1016/j.tws.2014.02.015>.
- Wang, W.H., Han, L.H., Li, W. and Jia, Y.H. (2014), "Behavior of concrete-filled steel tubular stub columns and beams using dune sand as part of fine aggregate", *Constr. Build. Mater.*, **51**, 352-363. <https://doi.org/10.1016/j.conbuildmat.2013.10.049>.
- Yang, Y.F. and Han, L.H. (2006), "Compressive and flexural behaviour of recycled aggregate concrete filled steel tubes (RACFST) under short-term loadings", *Steel Compos. Struct.*, **6**(3), 257-284. <http://dx.doi.org/10.12989/scs.2006.6.3.257>.
- Yang, Y.F. and Ma, G.L. (2013), "Experimental behaviour of recycled aggregate concrete filled stainless steel tube stub columns and beams", *Thin-Wall. Struct.*, **66**, 62-75. <https://doi.org/10.1016/j.tws.2013.01.017>.
- Yuan, F., Huang, H. and Chen, M., (2019). "Effect of stiffeners on the eccentric compression behaviour of square concrete-filled steel tubular columns", *Thin-Wall. Struct.*, **135**, 196-209. <https://doi.org/10.1016/j.tws.2018.11.015>.
- Yang, Y.F. (2015), "Modelling of recycled aggregate concrete-filled steel tube (RACFST) beam-columns subjected to cyclic loading", *Steel Compos. Struct.*, **18**(1), 213-233. <https://doi.org/10.12989/scs.2015.18.1.213>.
- Zhang, Y.B., Han, L.H., Zhou, K. and Yang, S. (2019), "Mechanical performance of hexagonal multi-cell concrete-filled steel tubular (CFST) stub columns under axial compression", *Thin-Wall. Struct.*, **134**, 71-83. <https://doi.org/10.1016/j.tws.2018.09.027>.
- Zhao, X.L. and Jaspert, J.P., (2005), "Width-to-thickness ratios for classification of tubular sections", *Proceedings of the 2005 Eurosteel Conference on Steel and Composite Structures (Volume-A)*, 183-190.
- Zhu, A., Zhang, X., Zhu, H., Zhu, J. and Lu, Y. (2017), "Experimental study of concrete filled cold-formed steel tubular stub columns", *J. Constr. Steel Res.*, **134**, 17-27. <https://doi.org/10.1016/j.jcsr.2017.03.003>.

CC